Spatial Multiomics Analysis Identifies SOCS1 as a Key Immune Checkpoint in T cell Tolerance Induction of HSCT

Ruifeng Li
Peking University
Huidong Guo
Peking University People's Hospital
Ming Wang
Peking University People's Hospital
Yingping Hou
Peking University
Shuoshuo Liu
Peking University People's Hospital
Ting Peng
Peking University People's Hospital
Xiangyu Zhao
Peking University People's Hospital
Liming Lu
Shanghai Jiaotong University
Yali Han
Peking University People's Hospital
Yiming Shao
Peking University People's Hospital
Ying-Jun Chang
Peking University People's Hospital https://orcid.org/0000-0002-6124-6050
Cheng Li
School of Life Sciences, Center for Bioinformatics, Center for Statistical Science, Peking University, Beijing https://orcid.org/0000-0002-1766-1409
Xiao-Jun Huang (xjhrm@medmail.com.cn)
Peking University People's Hospital

Article

Keywords: Hematopoietic Stem Cell Transplantation, Tolerance Profiles in Physiological State, Granulocyte Colony-stimulating Factor, Cytokine Signaling, Spatial Multiomics Analysis

Posted Date: February 15th, 2021

DOI: https://doi.org/10.21203/rs.3.rs-150508/v1

Abstract

Achieving T cell tolerance ensures superior clinical outcomes in hematopoietic stem cell transplantation (HSCT). However, the *in vivo* T cell tolerance profiles in physiological state need to be further delineated. Here, we characterized the gene expression profile in tolerant T cells which was induced in healthy donors by granulocyte colony-stimulating factor, a stem cell mobilizer extensively used in HSCT. We identified suppressor of cytokine signaling 1 (*SOCS1*) as an essential immune checkpoint for T cell tolerance in the mouse models and primary T cells in the HSCT context. Further spatial multiomics analysis characterized the distinct three-dimensional genome architecture and the gene regulatory network in tolerant T cells. We found STAT3 competes with CTCF and mediates the formation of a new chromatin loop between the *SOCS1* promoter and upstream super enhancers during the induction of T cell tolerance. This study identifies SOCS1 as a key immune checkpoint and potential immune target for improving outcome of patients with HSCT.

Introduction

T cell tolerance, which ensures that T cells can effectively eliminate foreign antigens while maintain hyporesponsive to self-antigens, promises superior clinical outcomes in transplantation and autoimmune diseases. Although hematopoietic stem cell transplantation (HSCT) became a curative therapy for a wide range of hematological malignancies, donor T cells failing to reach the tolerant state in host microenvironment leads to severe graft versus host disease (GVHD) and threatens the survival of patients after HSCT. Several strategies have been developed to induce tolerance and minimizing GVHD occurrence post-HSCT, such as blockade of costimulatory signals, transforming growth factor beta and regulatory T cells (Treg) [1, 2, 3].

Granulocyte colony-stimulating factor (G-CSF), initially identified as a growth factor for neutrophils, has been widely used as a mobilizer for stem/progenitor cells in HSCT settings. In the past two decades, increasing evidence has supported the critical role of recombinant human G-CSF in the induction of T cell tolerance, which is characterized by decreased proliferation and interleukin-2 production, in healthy HSCT donors [4, 5, 6]. Experimental evidence suggests that G-CSF is a strong immune regulator of T cells and directly modulates T-cell immune responses via its receptor on T cells [5, 7]. These data indicate that human tolerant T cells induced by G-CSF provide a platform to elucidate the essential genomic and epigenomic factors in maintaining T cell tolerance in HSCT context.

Previous studies have profiled gene expression patterns or key transcription factors (TFs) in the induction and maintaining of T cell tolerance under pathological conditions[8, 9, 10]. However, investigating gene expression alone provides limited information ignoring crucial role of regulatory networks. Moreover, few have investigated the potential role of chromatin reorganization in the induction of T cell tolerant state, especially under physiologic conditions. Recent advances in chromatin structure analytic technologies, including assays for transposase-accessible chromatin with high-throughput sequencing (ATAC-seq) and genome-wide chromosome conformation capture (Hi-C), enable delineating the profile of *trans*-acting

factors and *cis*-regulatory elements in chromatin reorganization[11, 12, 13]. These approaches help us investigate the chromatin state and 3D chromatin interactions of T cells from steady state to tolerant state under physiologic conditions.

In this study, we systematically investigated the dynamics of transcriptomes and 3D chromatin interaction coordinate in a physiologic T cell tolerance model established by treating healthy donors with G-CSF. We characterized the expression profile in the tolerant T cells and identified the essential role of SOCS1 in the induction and maintaining of T cell tolerance in HSCT. Furthermore, spatial multiomics analysis revealed the chromatin reorganization of T cell from steady state to tolerant state and we demonstrated transcription factor STAT3, acting as epigenetic coordinator in promoting SOCS1 expression level during the induction of T cell tolerance. Our study provides insights into transcriptomes and epigenetic modifications in T cell tolerance induction in HSCT.

Results

Tolerant state T cells exhibit distinct gene expression profiles and TF distributions.

T cell tolerance could be induced by *in vivo* application of G-CSF in both mice and humans [4, 5, 6]. We assessed the transcriptome, chromatin accessibility and 3D genome landscape of steady state $CD4^+$ and $CD8^+$ T cells ($CD4^+$ T_{ss} and $CD8^+$ T_{ss}, respectively) together with tolerant state $CD4^+$ and $CD8^+$ T cells ($CD4^+$ T_{tol} and $CD8^+$ T_{tol}, respectively) in human bone marrow (BM) (Fig. 1A and Fig. S1). Steady state and tolerant state T cells were distinct from each other both in $CD4^+$ and $CD8^+$ T cells, as shown in dendrograms generated using transcriptome data (Fig. 1B). Then we explored and validated genes that were differentially expressed during the induction of tolerance in human $CD4^+$ and $CD8^+$ T cells ($CD4^+$ T_{tol} and $CD8^+$ T_{tol}) by G-CSF. We found that $CD8^+$ T_{tol} cells differentially expressed multiple genes, such as SOCS1, PRDM1 and SEMA7A (Fig. 1C-D), compared to $CD8^+$ T_{ss} cells. We observed changes in a core set of genes, including suppressor of cytokine signaling 1 (SOCS1), PR/SET domain 1 (PRDM1), in a similar manner in $CD4^+$ T_{tol} and $CD8^+$ T_{tol} cells (Fig. 1C-D, and S2A-B). However, both $CD4^+$ T_{tol} and $CD8^+$ T_{tol} cells also exhibited changes in specific sets of genes. Notably, genes with $CD8^+$ T cell-based changes in expression included SEMA7A, whereas those with $CD4^+$ T cell-based changes included nuclear factor-κB inhibitor alpha (NFKBIA) (Fig. 1C-D, and S2A-B). Thus, although there is a clear transcriptomic change shared by both CD4 and CD8 lineages, there were also unique differentially expressed genes and TFs in $CD4^+$ and $CD8^+$ T cells during tolerance induction *in vivo*. CD8 T_{tol} cells showed a significant downregulation of genes related to cell activation (Fig. 1E), and CD4 T_{tol} cells showed downregulation of cytokine signaling genes (Fig. S2C). These results indicated T cells from G-CSF administrated healthy donors exhibited tolerance phenotype. Furthermore, we validated the direct upregulation of SOCS1 expression level by G-CSF in highly purified $CD3^+$ T cells from 7 independent heathy donor BM samples *in vitro*. The results showed that G-CSF stimulation led to a peak in SOCS1 mRNA production after 4 h of culture, followed by recovery after 72 h of culture (Fig. 1F, Fig. S3A-B). After cultured 72 h of $CD3^+$ T cells

with G-CSF stimulation *in vitro*, the G-CSFR expression level was significantly increased (Fig. S3C-D). Consistent with previous studies[7], IL-2 was decreased in the G-CSF treatment group which indicated that G-CSF suppressed differentiation of T cells to the Th1 type (Fig. 1G, Fig. S3E). These results demonstrated that G-CSF directly upregulated SOCS1 expression levels via GCSFR.

G-CSF loses its protective role in a GVHD mouse model in the absence of Socs1.

To investigate the role of SOCS1 regulation on T cell function during G-CSF induction of tolerance *in vivo*, we established a T cell-specific *Socs1* conditional knockout (cKO; LckCre-*Socs1*$^{fl/fl}$) mouse model. Consistent with previous studies[14], most cKO mice survived longer than 6 months. Occasionally, cKO mice developed dermatitis at 4 weeks (3 in 50 mice, Fig. S4A). There was slight splenomegaly in the cKO mice compared with *Socs1*$^{fl/fl}$ (WT) mice (Fig. S4B-C). Flow cytometry analysis showed that $CD3^+$ T cell were decreased in cKO mice compared with WT mice (Fig. S4D). The transposition of the CD4/CD8 ratio in cKO mice represents a decrease in $CD4^+$ T cells and an increase in $CD8^+$ T cells in cKO mice compared with WT mice (Fig. S4E). The ratio of naïve $CD4^+$ T cells was increased in the cKO mice compared with the WT mice (Fig. 2A-B). IFN-γ secretion in $CD4^+$ and $CD8^+$ T cells in cKO mice was increased compared with that in WT mice (Fig. 2C-D). These data suggested that loss *Socs1* might induce severe GVHD in the HSCT mouse model.

To validate this hypothesis, we examined the effect of losing *Socs1* in T cells on the protective role of G-CSF in a well-established murine GVHD model (C57BL/6 to BALB/c). Donor WT or cKO mice received 5 daily subcutaneous injections of either PBS or 5 μg human G-CSF, and spleens were harvested on day 6. BALB/c recipient mice received 8 Gy total body irradiation (TBI), and 3×10^6 T cells from the spleen were transplanted intravenously from the respective donors the following day. We transplanted 5×10^6 T cell-depleted bone marrow cells (TCD-BM) as protective cells from the WT PBS group donor mice to all groups of recipient mice. As shown in Fig. 2E, G-CSF prolonged the survival of WT mice compared with the PBS group (green vs. blue); however, G-CSF accelerated the death of GVHD mice in the cKO group (yellow vs. red). A validation experiment in which 5×10^6 TCD-BM and 2×10^6 T cells were transplanted from the spleen also indicated that G-CSF exacerbated GVHD and shortened the life span of cKO mice compared with WT mice (Fig. 2F). Flow cytometry analysis also showed that G-CSF inhibited CD62L expression levels in both WT and cKO mice (Fig. S4F-G), which is consistent with our previous studies in clinical samples.

We further investigated the G-CSF-administered donor-derived T cell phenotype in recipient mice in GVHD models. Compared with the WT mice, the naïve populations of both $CD4^+$ and $CD8^+$ T cells were increased in the cKO group (Fig. 2G-H). The proliferation ability of $CD4^+$ T cells from cKO mice was significantly increased compared with that of $CD4^+$ T cells from WT mice (Fig. 2I). Moreover, we transplanted 1×10^6 MLL-AF9-induced AML cells into nonirradiated WT or cKO mice to investigate T cell function in the context of leukemia. The results showed that the loss of *Socs1* in T cells prolonged survival in leukemic mice and delayed leukemia progression (Fig. 2J). This result indicated that losing

Socs1 might activate T cell function in the tumor environment. Taken together, these results demonstrated that Socs1 is the key mediator in G-CSF-induced T cell tolerance.

High expression levels of SOCS1 impairs T cell proliferation and decreases aGVHD occurrence after HSCT.

To further investigate the role of SOCS1 in maintaining T cell tolerance, we used lentivirus to overexpress SOCS1 in steady-state T cells and found that the SOCS1 expression level was increased approximately 30-fold in the SOCS1 overexpression group (SOCS1 OE) compared with the control group (CT) (Fig. 3A). High expression of SOCS1 inhibited T cell proliferation, and more T cells were blocked in the G0 stage in the SOCS1 OE group compared to the CT or noninfection control group (Fig. 3B). The proliferative ability of $CD4^+$ T cells was decreased in the SOCS1 OE group compared to the CT or noninfection group, while $CD8^+$ T cells showed no change (Fig. 3C-D, Fig. S5A). This result is consistent with the *in vivo* study in which the proliferation ability of $CD4^+$ T cells from *Socs1* cKO mice was increased compared with that of $CD4^+$ T cells from WT mice (Fig. 2I). Moreover, high SOCS1 expression in T cells also promoted TIGIT expression (Fig. 3E, Fig. S5B-C). There were no significant differences in the secretion of cytokines, such as IFN-γ, IL-2, IL-17, IL-4, and IL-10, by $CD4^+$ T and $CD8^+$ T cells between the SOCS1 OE group and CT group (Fig. 3F, Fig. S6A-C).

We further validated the relationship between the expression level of SOCS1 in T cells and aGVHD occurrence in patients after allo-HSCT. The results showed that there was a lower expression level of SOCS1 in the patients with aGVHD than in the patients without aGVHD at the same timepoint after allo-HSCT (Fig. 3G). This result indicated that a low expression level of SOCS1 might induce aGVHD after allo-HSCT.

G-CSF Regulates Target Gene Expression by Chromatin structure alteration.

Previous results identified SOCS1 as a key immune checkpoint for T cell tolerance, thus the regulatory network of SOCS1 needs to be further investigated. To explore the regulatory mechanism of SOCS1 during T cell tolerance induction, we performed transcription factor enrichment analysis in chromatin regions with differences in accessibility between $CD8^+$ T_{tol} and $CD8^+$ T_{ss} cells using ATAC-seq data [15]. The regions with high chromatin accessibility were located in promoter and distal intergenic and distinct in steady state and tolerant state T cells (Fig. S7A-B). We observed higher chromatin accessibility at the promoter and upstream elements of cell-type specific genes than at other regions in $CD4^+$ and $CD8^+$ T_{ss} (Fig. S7C-E), consistent with the characteristics of these two cell lineages [16]. These results highlight the feasibility and reliability of ATAC-seq in investigating the genome landscape and chromatin accessibility of human T cells. We found that TFs such as STAT3 were specifically activated in $CD8^+$ T_{tol} compared to $CD8^+$ T_{ss} cells (Fig. 4A). T cell activation related TFs such as JunB, AP-1 were suppressed in $CD8^+$ T_{tol} compared to $CD8^+$ T_{ss} cells (Fig. 4B). Differential expression of genes and differential activation of TFs including TXNIP and RUNX1 between $CD4^+$ T_{tol} and $CD4^+$ T_{ss} were observed (Fig. S7E-F). According to

the relationship between TFs and target genes [17], we plotted the network of upregulated genes and enhanced regulatory transcription factors in CD8 cells (Fig. 4C), which shows that SOCS1 is highly expressed and that the TF most strongly regulating SOCS1 is STAT3. We also identified a regulatory network of highly expressed genes and enhanced TFs in $CD4^+$ cells (Fig. S7G).

Next, we analyzed the spatial regulatory relationship between transcription factors and target genes which is 3D genome interaction maps of $CD4^+$ and $CD8^+$ T cells from steady state to tolerant state. We obtained high-resolution maps (5 kb) of the 3D genome structure, including A/B compartments, TAD structure and loop structure, of all the samples (Fig. 4D). The HiCRep SCC scores [18] of the Hi-C matrices showed that cells of different lineages have different 3D genome structures (Fig. 4E). The loop length of $CD4^+$ T_{ss} was significantly longer than that of $CD8^+$ T_{ss} (median length: CD4 T_{ss}, 210 kb; CD8 T_{ss}, 190 kb; Fig. 4F-G). This finding indicates that the chromatin structure of $CD4^+$ T cells is more variable than that of $CD8^+$ T cells at the level of loops during the induction of tolerance.

The switch of A/B compartments from steady-state T cells to tolerant cells is shown for chromosome 10 in Fig. S8A. Approximately 7.4% and 7.3% of the genome regions in $CD4^+$ and $CD8^+$ T cells, respectively, switched from compartment A to B and were associated with downregulated gene expression after tolerance induction. Meanwhile, 6.6% and 4.5% of the genome regions in $CD4^+$ and $CD8^+$ T cells, respectively, switched from compartment B to A and were associated with upregulated gene expression (Fig. S8B-C). The TAD boundaries were more accessible and were enriched with CTCF and H3K27ac signals [13] (Fig. S8D). We found that most of the TAD boundaries (> 90%) are conserved and that the length of the TADs decreased slightly in the tolerant $CD4^+$ and $CD8^+$ T cells compared to the steady-state cells (Fig. S8E-F).

We demonstrated that more than 53% of the genes upregulated in CD8 T_{tol} cells compared with $CD8^+$ T_{ss} cells, including SOCS1, PRDM1, and KLF9, are located in the loop anchor regions (Fig. 4H, $P < 1e\text{-}16$). These observations showed that most of the differentially expressed genes may contact distal cis-regulatory elements via chromatin loops during the *in vivo* induction of human T cell tolerance. We found 7,481 chromatin loops in $CD8^+$ T_{ss} and 6,186 chromatin loops in $CD8^+$ T_{tol} cells, with 4,786 chromatin loops appearing in both (Fig. 4I). Compared with those in $CD8^+$ T_{ss} cells, STAT3 and PRDM1 motifs were enriched in the gained loop anchors and were highly expressed in $CD8^+$ T_{tol} cells, which is consistent with the ATAC-seq results (Fig. 4A, 4J). This suggests that STAT3 may be a structural protein that mediates the gain of chromatin loops. The lost loop anchor-enriched TFs included ZNF416 and TCF4 in $CD8^+$ T_{tol} cells (Fig. 4J, Fig. S8G).

Association of STAT3 with SOCS1 Expression in Tolerant T Cells

We next explored the regions of spatial interaction with the promoter of *SOCS1* and determined which transcription factors bind to these regions. On chromosome 16, the SOCS1 gene is located within one TAD in $CD8^+$ T_{ss} cells (Fig. 5). Then, we investigated the chromatin spatial structure, histone modification and TF binding sites around the *SOCS1* gene. The genome-browser view of CTCF and STAT3 binding sites suggests that the CTCF protein mediates the interaction between the SOCS1 locus and the downstream chromatin region, and STAT3 proteins mediate the interaction between SOCS1 and upstream super enhancers. From Hi-C data, the interaction between the SOCS1 locus and downstream heterochromatin is weakened, and the interaction between SOCS1 and upstream super enhancers is enhanced in $CD8^+$ T_{tol} cells compared to $CD8^+$ T_{ss} cells (Fig. 5). These results suggest that a new association of STAT3 with SOCS1 expression emerged during the *in vivo* induction of human T cell tolerance. In support of this hypothesis, genome-wide statistics showed that genes with long-range interactions with heterochromatin tended to be expressed at low levels, while genes with long-range interactions with enhancers tended to be highly expressed (Fig. S8H).

STAT3 mediates the spatial interaction between enhancers and promoters in the whole genome.

To investigate whether STAT3 competes with CTCF in regulating target genes, we performed ChIP-seq and CUT&Tag experiments to detect the colocalization of STAT3 and CTCF. For example, many of the binding sites of STAT3 and CTCF are colocalized in and around SOCS1 (Fig. 6A) and TXNIP (Fig. 6B), which are upregulated after G-CSF mobilization. Furthermore, STAT3 and CTCF colocalized in the whole genome analysis of human CD8 T cells and GM12878 cell lines (Fig. 6C-E and Fig. S9A-D). There was a significant overlap between the CTCF peaks and the STAT3 peaks in CD8 T cells, as shown by Venn diagram (P< 1e-10, Fig. 6F). The peaks of STAT3 binding are enriched in promoter and enhancer regions (Fig. 6G-H). Then, we classified the peaks of STAT3 binding into promoter regions or enhancer regions (Fig. 6H and Fig. S9E-G), and there is a significant spatial interaction between the promoter regions and enhancer regions (Fig. 6I-J). These results strongly suggest that the STAT3 complex is involved in enhancer and promoter interactions. Consistent with our observation, previous studies showed STAT3 could regulate chromatin topology and mediate transcription during T cell differentiation [19, 20, 21]. STAT4 binding in the genome contributes to the specification of the nuclear architecture around *Ifng* during Th1 differentiation[22]. Furthermore, we observed both CTCF and STAT3 foci in the nuclei of Jurkat cells by immunofluorescence staining (Fig. S9H). Collectively, these results suggest that a STAT3-mediated enhancer-promoter interaction induces SOCS1 expression during the *in vivo* induction of T cell tolerance (Fig. S9I).

Furthermore, we detected STAT3 protein levels in SOCS1 overexpressed Jurkat T cell line. The results showed that a high SOCS1 expression level inhibited the phosphorylation of STAT3 (Fig. S10A-B). Moreover, the Western blotting results in the spleen cells from mice with T cell-specific *Socs1* knock out showed that the phosphorylation of STAT3 was upregulated when Socs1 expression was inhibited (Fig. S10C-D). These results indicated that SOCS1 regulated the activation of STAT3 through a negative feedback loop.

Discussion

Here, we have taken advantage of a well-defined physiologic T cell tolerant state which is induced by G-CSF involving multiomics analysis revealed the chromatin reorganization during T cell tolerance induction. Unsupervised clustering of accessible chromatin regions, specifically distal elements, groups individual cell types with high cluster purity, suggesting that these distal regulatory elements precisely define T cell immunological characteristics during the induction of tolerance. In addition, changes in the 3D genome compartment status might influence the accessibility of genomic regions to transcription factors or other regulatory proteins, which could be particularly important for certain subsets of genes. Furthermore, we identified SOCS1 as a key immune checkpoint in the induction and maintaining of T cell tolerance in HSCT. Integration of multiomics data enabled us to identify a novel regulatory model for SOCS1 expression during T cell tolerance induction (Fig. 7). The methodologies developed here might have important implications for addressing immunological profiles, such as those of dendritic cells and B cells, in other contexts of tolerance induction [9] as well as in cellular therapy.

SOCS1 belongs to classic negative feedback inhibitor family and plays an indispensable role in attenuating IFN-γ signaling[23, 24]. Consistent with previous studies, we also found *Socs1* cKO mice showed aberrant CD4/CD8 ratio, which is indicated *Socs1* involved in T-cell development in the thymus[25, 26]. Interestingly, although we observed enlarged spleen in *Socs1* cKO mice as previous studies reported[14, 27], there is no statistical significance and cKO mice occasionally developed dermatitis. The *Socs1* cKO mice didn't develop severe inflammatory symptom in steady state. However, in the GVHD transplantation mouse models, G-CSF treated *Socs1* cKO donor mice group developed more severe GVHD and shortened lifespan compared with PBS treated *Socs1* cKO donor mice group (Fig. 2E-F). These results indicated the essential role of *Socs1* in G-CSF induced T cell tolerance. Moreover, clinical data showed that there is low expression level of SOCS1 in T cells from patients with GVHD compared those without GVHD at the same period after HSCT (Fig. 3G). It might indicate SOCS1 involved in the maintaining of T cell tolerance in HSCT. Recently published work revealed *SOCS1* haploinsufficiency causes autoimmune diseases and related to cytokine hypersensitivity of immune cells [28]. Taken together, these findings strongly indicated SOCS1 as a potential immune target for the clinical therapy of autoimmune diseases and transplantation.

In addition of SOCS1, we also found classical T cell tolerance regulators involved in G-CSF induced tolerant T cells. In $CD8^+$ T_{tol} cells, the expression of AP-1 was significantly downregulated, accompanied by the upregulation of NFATC2. In $CD4^+$ T_{tol} cells, the expression of Jun was also significantly downregulated, accompanied by the upregulation of NFKBIA (Fig. 1C-D and Fig. S2A-B). Previous studies showed that T cell anergy could be induced if the interaction of NFAT with its transcriptional partner AP-1 (Fos/Jun) was prevented [10]. We also found an immune tolerance mediator, B lymphocyte-induced maturation protein-1 (Blimp-1) which is a zinc finger-containing transcriptional repressor encoded by PRDM1 [29, 30], was upregulated in $CD4^+$ T_{tol} and $CD8^+$ T_{tol} cells compared with $CD4^+$ T_{ss} and $CD8^+$ T_{ss}

cells, respectively (Fig. 1D and Fig. S2B). Overall, our study confirmed the G-CSF induced T cell tolerance partially via classical tolerance regulator TFs.

From the spatial multiomic data analysis, we observed a STAT3-mediated enhancer/promoter interaction for SOCS1 gene expression and proposed a novel model in which STAT3 could replace CTCF and form new chromatin loops, leading to the expression of SOCS1 (Fig. 7). Similarly, another TF NF-κB has been reported could compete with CTCF, forming a new loop and enhancing PD-L1 expression [31]. Previous studies also showed STAT3 could regulate chromatin topology and mediate transcription during T cell differentiation [19, 20, 21]. These data suggest that STAT3 activating downstream target genes during T cell activation and tolerance might via reorganizing the chromatin structure and involved in distal regulatory elements.

In summary, based on physiologic T cell tolerance model and multiomics analyses, we established a platform for discovering novel genes and TFs that induce immune tolerance. Our data resource will serve as a valuable tool for the community to further elucidate the gene regulatory networks controlling the induction of human T cell tolerance. In addition, the essential role of SOCS1 in the induction and maintaining of T cell tolerance suggests that this gene could be a potential target for clinical therapy.

Materials And Methods

T cell isolation and culture

Human bone marrow mononuclear cells (BMMCs) were isolated from the BM of healthy donors before and after *in vivo* G-CSF application by Ficoll density centrifugation. $CD3^+$ T cells were purified by positive selection (CD3 MACS MultiSort beads; Miltenyi Biotec, Bergische Gladbach, Germany). The isolated $CD3^+$ T cells were cultured in IMDM (Gibco, Invitrogen, Carlsbad, CA) containing 10% BIT 9500 (Stemcell Technologies, Vancouver, CA) and stimulated with Dynabeads Human T-Activator CD3/CD28 (Gibco, Invitrogen, Carlsbad, CA). The study was approved by the Institutional Review Board of Peking University. Written informed consent was obtained from all healthy donors in accordance with the Declaration of Helsinki.

In vitro**stimulation with G-CSF**

$CD3^+$ T cells isolated from healthy donors were incubated with G-CSF (100 ng/ml) for 4 h or 72 h at 37°C and 5% CO_2.

Mice

LckCre-*Socs1*$^{fl/fl}$ (T cell-specific Socs1-cKO) and *Socs1*$^{fl/fl}$ (littermate control; WT) mice (sex- and age-matched) were used. All mice were maintained in the specific pathogen-free animal facility of Peking University People's Hospital. All experiments were performed according to the National Institutes of Health's Guide for the Care and Use of Laboratory Animals.

GVHD mouse models

Acute GVHD was induced as described previously [32]. In brief, donor cKO or WT mice (C57BL/6 background) were subcutaneously injected with G-CSF (250 μg/kg daily) or the same volume of PBS for 5 days. These donor mice were sacrificed the day after the last dose was given. Splenic T cells were isolated from G-CSF- or PBS-treated donor mice by negative selection using a Pan T Cell Isolation Kit II (Miltenyi-Biotec, Germany), and the obtained cells had a purity of > 95%. BM cells from PBS-treated WT mice were T cell-depleted with anti-90.2 MicroBeads (Miltenyi-Biotec). Once splenic T cells and TCD-BM cells were purified, they were injected into the tail veins of prepared recipient mice. BALB/c hosts were subjected to total body irradiation from a [^{60}Co] source (8 Gy). They were randomly grouped.

Leukemia mouse models

The generation of the MLL-AF9 leukemia mouse model was described in detail previously [33]. Leukemia cells were thawed, and live cells were counted by staining with trypan blue. The ratio of GFP^+ cells was detected with flow cytometry. A total of 1×10^6 live GFP^+ MLL-AF9 leukemia cells were transplanted into nonirradiated recipient mice, and mouse survival was monitored.

Lentivirus-mediated SOCS1 overexpression in T cells

The SOCS1-overexpressing lentivirus was purchased from Sangon Biotech (Shanghai, China). $CD3^+$ T cells were prestimulated for 24 h with Dynabeads Human T-Activator CD3/CD28 in IMDM containing 10% BIT 9500, and rhIL-2 was added at a dose of 100 U/ml. After 24 h, the cells were transduced with thawed lentiviruses that were added directly to the plate. Then, 6 μg/ml polybrene (Sigma, USA) was added. The cells were incubated for another 24 h at 37°C and 5% CO_2, and fresh medium was changed. GFP^+ cells were isolated after a 72-h infection and cultured in IMDM containing 10% BIT 9500 with rhIL-2 routinely used.

Flow cytometric analysis

Surface staining was performed with directly conjugated monoclonal antibodies for 20 min at room temperature for human samples. The cells were washed and resuspended in phosphate-buffered saline (PBS) before flow cytometric analysis. The monoclonal antibodies used were anti-human CD4-Percp-Cy5.5/APC-H7, CD8-APC-R700/V500, PD-1-PE-Cy7, Tim-3-APC, Tigit-BV605, 2B4-AF700, and CD160-PE (BD Bioscience San Diego, CA, USA). Intracellular staining was carried out by using a fixation/permeabilization kit (BD Bioscience) after resuspension according to the manufacturer's instructions. Ki-67-PE (BD Pharmingen) was added and incubated for 20 min at room temperature.

We stained the surfaces of mouse samples with direct-conjugated monoclonal antibodies for 30 min at 4°C. After incubation, the cells were washed and resuspended in phosphate-buffered saline before flow cytometry analysis. The monoclonal antibodies used were anti-mouse CD3-Percp, CD4-APC-H7, CD8-FITC, CD44-PE-Cy7, and CD62L-APC (BD Bioscience San Diego, CA, USA).

Cytokine detection by flow cytometry

T cells were stimulated with Dynabeads Human/Mouse T-Activator CD3/CD28 (Gibco, Invitrogen, Carlsbad, CA). After 72 h of culture, GolgiPlug (BD Pharmingen, San Diego, CA, USA) was added for 4 h. Cells were harvested for surface staining as described above. Intracellular staining was carried out by using a fixation/permeabilization kit (BD Bioscience) after resuspension according to the manufacturer's instructions. For human samples, IL-2-V450, IFN-γ-BV510, IL-17-PE, IL-4-APC, and IL-10-PE (BD Pharmingen) were added and incubated for 20 min at room temperature. For mouse samples, IFN-γ-PE (BD Pharmingen) was added and incubated for 30 min at 4°C.

T-cell proliferation analysis (CSFE)

$CD3^+$ spleen T cells were isolated with a pan T cell isolation kit (Miltenyi-Biotec, Germany). The purified T cells were stained with CFSE (BD Bioscience) to achieve a final concentration of 5 μM for 5 min at 37°C and washed twice with complete medium with 10% FBS. Labeled T cells (2×10^5 cells/well) were stimulated with CD3/28 beads in flat-bottomed 96-well plates in complete RPMI. After 96 h, cells were harvested, stained with CD4-APC-H7 and CD8-APC-R700 (BD Bioscience), and then analyzed by flow cytometry.

RT-PCR

RNA was extracted using the RNeasy Mini Kit (Qiagen, 74106) according to the manufacturer’s protocol. For quantitative PCR, first strand synthesis was performed using a cDNA reverse transcription kit (TaKaRa, RR047A) according to the manufacturer’s protocol. Quantitative PCR assays were performed in 96-well MicroAmp Fast Optical 96-Well Reaction Plates (Applied Biosystems, 4344904) using SYBR Green (Roche, 04913914001). Signals were detected using a 7500 Real-Time PCR System (Applied Biosystems). Target gene cycle numbers were normalized to the housekeeping gene 18S to obtain the ΔCT values. The $2^{-\Delta\Delta CT}$ method was used. The primer sequences were as follows: SOCS1 forward: 5'-CACGCACTTCCGCACATTC-3'; SOCS1 reverse: 5'-TAAGGGCGAAAAAGCAGTTCC-3'; human 18S forward: 5'-ACCGATTGGATGGTTTAGTGAG-3'; and human 18S reverse: 5'-CCTACGGAAACCTTGTTACGAC-3'.

RNA-seq experiments and analysis

Total mRNA with a polyA tail was extracted and reverse transcribed to cDNA for sequencing. Three biological repeats were performed for each sample, and 20 million reads were sequenced for each repeat. The sequenced reads were mapped to the human reference genome (hg19) by TopHat2 [34], and gene expression was quantified by Cufflinks [35]. We used RStudio software for the downstream statistical analyses.

ATAC-seq experiments and analysis

The ATAC-seq experiment was performed following Buenrostro’s protocol [15]. Two biological repeats were used for each sample, and 20 million reads were sequenced for each repeat. The sequenced reads were

mapped to the human reference genome (hg19) by Bowtie2 [34], and peak signals were quantified by MACS2 and deepTools. We used RStudio software for the downstream statistical analyses.

Hi-C experiments

The cells were resuspended in fresh PBS. Cell counts were performed. Then, a cell suspension with a final concentration of $1x10^6$ cells per 1 ml of PBS was prepared. A total of $1 x 10^6$ cells was isolated and crosslinked with 1% formaldehyde for 10 min at room temperature, and then, 2.5 M glycine solution was added to a final concentration of 0.2 M. Then, the cells were collected, flash-frozen in liquid nitrogen and stored at -80°C. The Hi-C experiment was performed following the in situ Hi-C protocol [13].

Hi-C data analysis

We performed read mapping and filtering of the Hi-C data following previous methods [36]. All Hi-C sequencing reads were mapped to the human reference genome (hg19) using Bowtie2 [37]. The two ends of the paired-end reads were mapped independently using the first 36 bases of each read. We filtered out redundant and nonuniquely mapped reads and kept the reads within 500 bp upstream of enzyme cutting sites (Mbol) for size selection. We used the iterative correction and eigenvector decomposition (ICE) method [38] to normalize raw interaction matrices.

A/B compartment analysis

We used ICE-normalized interaction matrices at 500 kb resolution to detect chromatin compartment types with the R package HiTC [39]. Positive or negative values of the first principal component separated the chromatin regions into two spatially segregated compartments. The compartment with a higher gene density was assigned as the A compartment, and the other compartment was assigned as the B compartment [40].

TAD analysis

We used ICE-normalized interaction matrices at 40 kb resolution to call TAD by a Perl script, matrix2insulation.pl (https://github.com/blajoie/crane-nature-2015). A higher resolution was possible because TADs are smaller than A/B compartments. Insulation scores (IS) were calculated for each chromosome bin, and the valleys of the IS identified the TAD boundaries. TADs smaller than 200 kb or located in telomeres/centromeres were filtered out as in previous methods [41]. In comparisons of TADs between two cell lines, at least 70% overlap between two TADs was considered to indicate TAD conservation [42]. We used BEDtools with the option of “intersectBed − f 0.70 − r” to identify conserved TADs [43].

Gene ontology analysis

We used DAVID Bioinformatics Resources 6.7 for Gene Ontology analysis [44]. The set of all human genes was used as the background gene list.

Chromatin immunoprecipitation

Jurkat cells were fixed in 1% formaldehyde (Sigma-Aldrich, F8775) for 10 min at 37°C. Subsequently, glycine was added to 125 mM and incubated at 37°C for 5 min at 37°C. Next, the cells were pelleted and washed twice with cold PBS. The pellets were stored at − 80°C until use.

Nuclei from 10 M cells per ChIP-seq were extracted, and chromatin was sonicated with a Bioruptor Sonication Device. Immunoprecipitation reactions were performed overnight with STAT3 (Cell Signaling Technology, 9139S, MA), H3K27ac or CTCF (ABclonal, A1133, China) antibodies. The next morning, antibodies and chromatin were captured using Protein G Dynabeads (Thermo Fisher). The material was washed, eluted and treated with RNase A for 30 min at 37°C and proteinase K for 3 h at 65°C.

Library preparation and sequencing

Library preparation from ChIP-seq DNA was performed using the Ultra II Library Prep Kit (NEB E7103L) and Multiplex Oligos for Illumina (NEB E7335L) and sequenced on an Illumina NextSeq 2500 instrument (150 base pairs single end).

ChIP-seq data processing, heat map generation, and edgeR analysis

H3K27ac, CTCF, and STAT3 ChIP-seq analyses were performed with an average range of 20–25 × 10^6 reads per independent ChIP-seq experiment. ChIP-seq reads were mapped to the hg19 genome with Bowtie2 using default parameters. Aligned reads were filtered for a minimum MAPQ of 30, and duplicates were removed using SAMtools. Signal tracks were generated by first using BEDTools to produce bedGraph files scaled to 10 million reads per data set. Then, the UCSC Genome Browser utility bedGraphToBigWig was used with default parameters to generate bigwig files. Peaks were called using MACS2 with default parameters. Heat maps of the ChIP-seq signal profiles were generated with the HOMER (http://biowhat.ucsd.edu/homer/index.html) tool annotatePeaks with the following parameters: -ghist 50, -size 10000. ChIP-seq peaks exhibiting differential H3K27ac or STAT3 signals across the time course were identified using edgeR, similar to the process described above.

CUT&Tag experiments and analysis

The CUT&Tag experiments were performed as previously described [45] (Vazyme TD901 kit) to generate DNA libraries derived from human CD8 T_{ss} cells. We used the SEACR peak caller (http://seacr.fredhutch.org), which was expressly designed for CUT&RUN and CUT&Tag data, to call peaks.

Code and data

All essential codes used for the analysis are available at GitHub (https://github.com/ChengLiLab/T_cell_tolerance). The raw sequencing data generated by this project were deposited at the Genome Sequence Archive (GSA, http://gsa.big.ac.cn) with accession number PRJCA002316.

Declarations

Conflict of Interest

The authors declare no conflicts of interest.

Author contributions

X.-J.H., C.L., and Y.-J.C. designed the study; R.-F.L. and H.-D.G. collected data; R.-F.L., H.-D.G., Y.-J.C., C.L., and X.-J.H. analyzed the data and drafted the manuscript; and all authors contributed to data interpretation and manuscript preparation and approved the final version.

Acknowledgements

This work was partly supported by grants from the National Key Research and Development Program of China (2017YFA0104500), the Beijing Municipal Science and Technology Commission (Z181110009618032), the National Natural Science Foundation of China (Grant Nos. 81670168, 81621001, 81530046, and 81770189), the Beijing Municipal Natural Science Foundation (Grant No. 7204319), and the Key Program of the National Natural Science Foundation of China (Grant No. 81230013). The CAMS Innovation Fund for Medical Sciences (CIFMS) (Grant No. 2019-I2M-5-034) and the Fundamental Research Funds for the Central Universities also provided funding. R.L. and C.L. were supported by the National Natural Science Foundation of China (31871266), the Chinese National Key Research and Development Program of China (2016YFA0100103), and NSFC Key Research Grant 71532001. Part of the data analysis was performed on the High-Performance Computing Platform of the Center for Life Sciences, Peking University. We thank Shanghai Jiayin Biotechnology, Ltd., for their help and suggestions for the ChIP-seq and CUT&Tag experiments. We thank all the faculty members who participated in these studies.

References

1. Wu SR, Reddy P. Tissue tolerance: a distinct concept to control acute GVHD severity. *Blood* **129**, 1747–1752 (2017).
2. Handel AE, Irani SR, Hollander GA. The role of thymic tolerance in CNS autoimmune disease. *Nat Rev Neurol* **14**, 723–734 (2018).
3. Zhao Y, Li X. Cross-immune tolerance: conception and its potential significance on transplantation tolerance. *Cell Mol Immunol* **7**, 20–25 (2010).
4. Jun HX, Jun CY, Yu ZX. In vivo induction of T-cell hyporesponsiveness and alteration of immunological cells of bone marrow grafts using granulocyte colony-stimulating factor. *Haematologica* **89**, 1517–1524 (2004).

5. MacDonald KP, *et al.* Modification of T cell responses by stem cell mobilization requires direct signaling of the T cell by G-CSF and IL-10. *J Immunol* **192**, 3180–3189 (2014).
6. Rutella S, Zavala F, Danese S, Kared H, Leone G. Granulocyte colony-stimulating factor: a novel mediator of T cell tolerance. *J Immunol* **175**, 7085–7091 (2005).
7. Franzke A, *et al.* G-CSF as immune regulator in T cells expressing the G-CSF receptor: implications for transplantation and autoimmune diseases. *Blood* **102**, 734–739 (2003).
8. Safford M, *et al.* Egr-2 and Egr-3 are negative regulators of T cell activation. *Nat Immunol* **6**, 472–480 (2005).
9. Lynn RC, *et al.* c-Jun overexpression in CAR T cells induces exhaustion resistance. *Nature* **576**, 293–300 (2019).
10. Martinez GJ, *et al.* The transcription factor NFAT promotes exhaustion of activated CD8(+) T cells. *Immunity* **42**, 265–278 (2015).
11. Calderon D, *et al.* Landscape of stimulation-responsive chromatin across diverse human immune cells. *Nat Genet* **51**, 1494–1505 (2019).
12. Philip M, *et al.* Chromatin states define tumour-specific T cell dysfunction and reprogramming. *Nature* **545**, 452–456 (2017).
13. Rao SS, *et al.* A 3D map of the human genome at kilobase resolution reveals principles of chromatin looping. *Cell* **159**, 1665–1680 (2014).
14. Takahashi R, *et al.* SOCS1 is essential for regulatory T cell functions by preventing loss of Foxp3 expression as well as IFN-{gamma} and IL-17A production. *J Exp Med* **208**, 2055–2067 (2011).
15. Buenrostro JD, Giresi PG, Zaba LC, Chang HY, Greenleaf WJ. Transposition of native chromatin for fast and sensitive epigenomic profiling of open chromatin, DNA-binding proteins and nucleosome position. *Nature methods* **10**, 1213–1218 (2013).
16. Kioussis D, Ellmeier W. Chromatin and CD4, CD8A and CD8B gene expression during thymic differentiation. *Nat Rev Immunol* **2**, 909–919 (2002).
17. Yan Z, *et al.* Integrative analysis of gene and miRNA expression profiles with transcription factor-miRNA feed-forward loops identifies regulators in human cancers. *Nucleic Acids Res* **40**, e135 (2012).
18. Yang T, *et al.* HiCRep: assessing the reproducibility of Hi-C data using a stratum-adjusted correlation coefficient. *Genome Res* **27**, 1939–1949 (2017).
19. Zhao Y, Zeng C, Tarasova NI, Chasovskikh S, Dritschilo A, Timofeeva OA. A new role for STAT3 as a regulator of chromatin topology. *Transcription* **4**, 227–231 (2013).
20. Tripathi SK, *et al.* Genome-wide Analysis of STAT3-Mediated Transcription during Early Human Th17 Cell Differentiation. *Cell Rep* **19**, 1888–1901 (2017).
21. Li P, *et al.* STAT5-mediated chromatin interactions in superenhancers activate IL-2 highly inducible genes: Functional dissection of the Il2ra gene locus. *Proc Natl Acad Sci U S A* **114**, 12111–12119 (2017).

22. Hakim O, Sung MH, Nakayamada S, Voss TC, Baek S, Hager GL. Spatial congregation of STAT binding directs selective nuclear architecture during T-cell functional differentiation. *Genome Res* **23**, 462–472 (2013).
23. Ilangumaran S, Bobbala D, Ramanathan S. SOCS1: Regulator of T Cells in Autoimmunity and Cancer. *Curr Top Microbiol Immunol* **410**, 159–189 (2017).
24. Palmer DC, Restifo NP. Suppressors of cytokine signaling (SOCS) in T cell differentiation, maturation, and function. *Trends Immunol* **30**, 592–602 (2009).
25. Catlett IM, Hedrick SM. Suppressor of cytokine signaling 1 is required for the differentiation of CD4 + T cells. *Nat Immunol* **6**, 715–721 (2005).
26. Yoshimura A, Ito M, Chikuma S, Akanuma T, Nakatsukasa H. Negative Regulation of Cytokine Signaling in Immunity. *Cold Spring Harb Perspect Biol* **10**, (2018).
27. Chong MM, *et al.* Suppressor of cytokine signaling-1 is a critical regulator of interleukin-7-dependent CD8 + T cell differentiation. *Immunity* **18**, 475–487 (2003).
28. Hadjadj J, *et al.* Early-onset autoimmunity associated with SOCS1 haploinsufficiency. *Nat Commun* **11**, 5341 (2020).
29. Martins GA, Cimmino L, Liao J, Magnusdottir E, Calame K. Blimp-1 directly represses Il2 and the Il2 activator Fos, attenuating T cell proliferation and survival. *J Exp Med* **205**, 1959–1965 (2008).
30. Kallies A, *et al.* Transcriptional repressor Blimp-1 is essential for T cell homeostasis and self-tolerance. *Nat Immunol* **7**, 466–474 (2006).
31. Chen H, *et al.* A Pan-Cancer Analysis of Enhancer Expression in Nearly 9000 Patient Samples. *Cell* **173**, 386–399 e312 (2018).
32. Zhou Y, *et al.* Th2 polarization in target organs is involved in the alleviation of pathological damage mediated by transplanting granulocyte colony-stimulating factor-primed donor T cells. *Sci China Life Sci*, (2020).
33. Guo H, *et al.* PBX3 is essential for leukemia stem cell maintenance in MLL-rearranged leukemia. *Int J Cancer* **141**, 324–335 (2017).
34. Kim D, Pertea G, Trapnell C, Pimentel H, Kelley R, Salzberg SL. TopHat2: accurate alignment of transcriptomes in the presence of insertions, deletions and gene fusions. *Genome biology* **14**, R36-R36 (2013).
35. Trapnell C, *et al.* Transcript assembly and quantification by RNA-Seq reveals unannotated transcripts and isoform switching during cell differentiation. *Nature biotechnology* **28**, 511–515 (2010).
36. Jin F, *et al.* A high-resolution map of the three-dimensional chromatin interactome in human cells. *Nature* **503**, 290–294 (2013).
37. Langmead B, Salzberg SL. Fast gapped-read alignment with Bowtie 2. *Nature methods* **9**, 357–359 (2012).
38. Imakaev M, *et al.* Iterative correction of Hi-C data reveals hallmarks of chromosome organization. *Nature methods* **9**, 999–1003 (2012).

39. Servant N, *et al.* HiTC: Exploration of high-throughput 'C' experiments. *Bioinformatics* **28**, 2843–2844 (2012).
40. Barutcu AR, *et al.* Chromatin interaction analysis reveals changes in small chromosome and telomere clustering between epithelial and breast cancer cells. *Genome biology* **16**, 214 (2015).
41. Crane E, *et al.* Condensin-driven remodelling of X chromosome topology during dosage compensation. *Nature* **523**, 240–244 (2015).
42. Taberlay PC, *et al.* Three-dimensional disorganisation of the cancer genome occurs coincident with long range genetic and epigenetic alterations. *Genome research* **April 8**, gr.201517.201115-gr.201517.201115 (2016).
43. Quinlan AR, Hall IM. BEDTools: A flexible suite of utilities for comparing genomic features. *Bioinformatics* **26**, 841–842 (2010).
44. Huang DW, Sherman BT, Lempicki RA. Bioinformatics enrichment tools: Paths toward the comprehensive functional analysis of large gene lists. *Nucleic acids research* **37**, 1–13 (2009).
45. Kaya-Okur HS, *et al.* CUT&Tag for efficient epigenomic profiling of small samples and single cells. *Nat Commun* **10**, 1930 (2019).

Figures

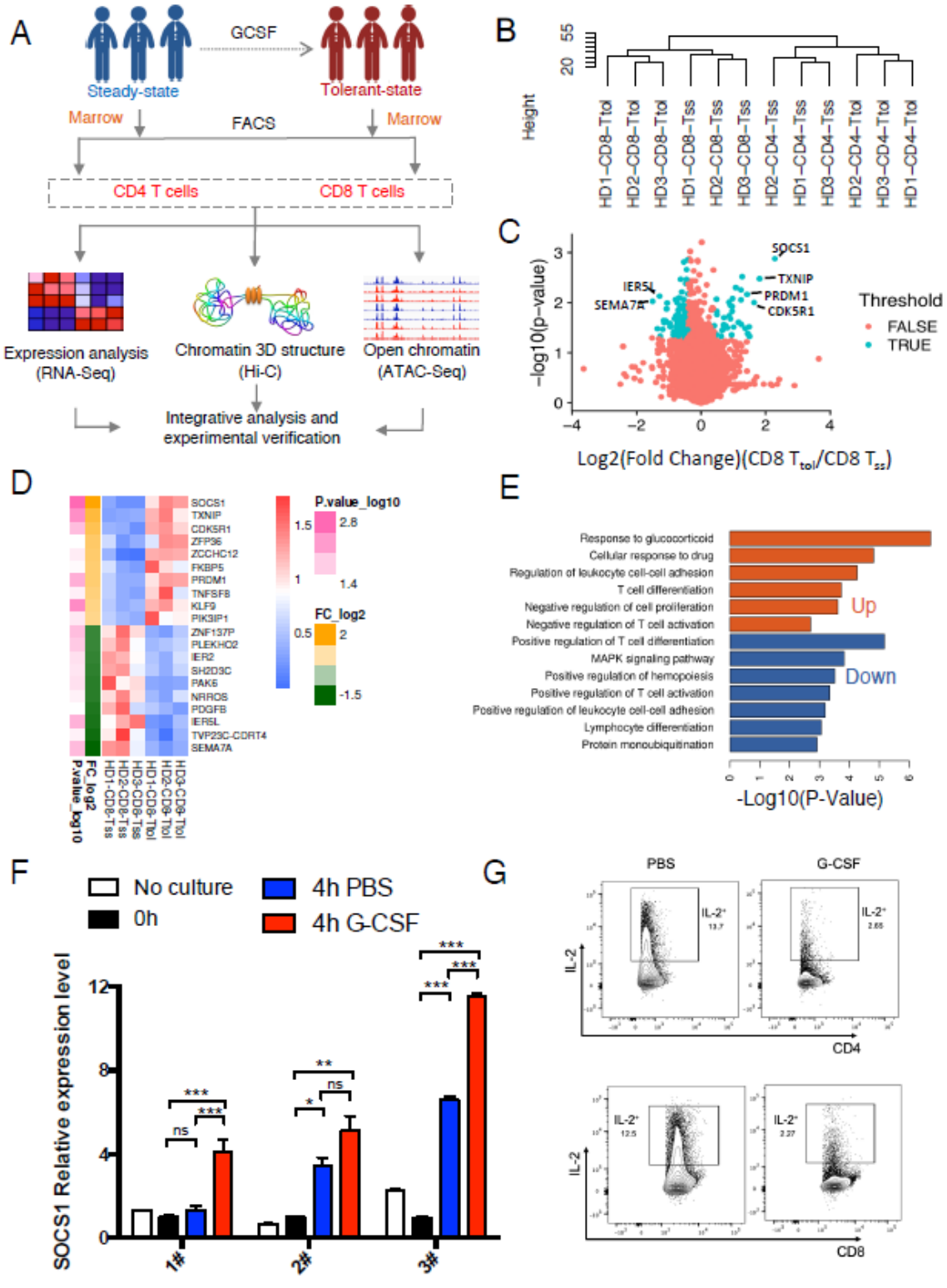

Figure 1

Gene expression profiles and TF distributions in tolerant T cells. (A) Outline of the experiments and analyses in this study. We performed in situ Hi-C, RNA-seq and ATAC-seq experiments on paired T cells (CD4 and CD8) from three healthy donors before and after G-CSF mobilization in vivo. (B) Unsupervised hierarchical clustering of the transcriptome (top 1000 genes with the largest difference between steady-state and tolerant-state cells). (C) Volcano plot comparing CD8 Tss and Ttol. The X-axis shows the fold

change (log2). Among the genes, 54 genes were significantly upregulated, and 78 genes were significantly downregulated. (D) The top ten genes with most upregulated and most downregulated expression in CD8 Ttol compared with CD8 Tss were identified (red: higher expression; blue: lower expression). (E) Gene pathway enrichment analysis for the upregulated (red) and downregulated (blue) genes in CD8 Ttol cells. (F) The expression level of SOCS1 in G-CSF-stimulated CD3+ T cells at 4 h from 3 independent healthy donors. Error bars represent the mean ± SEM values from 3 independent experiments. One-way ANOVA, *$p<0.05$, **$p < 0.01$, ***$p < 0.001$. (G) Flow cytometric analysis of IL-2 secretion in G-CSF-stimulated CD3+ T cells at 72 h from 7 independent healthy donors.

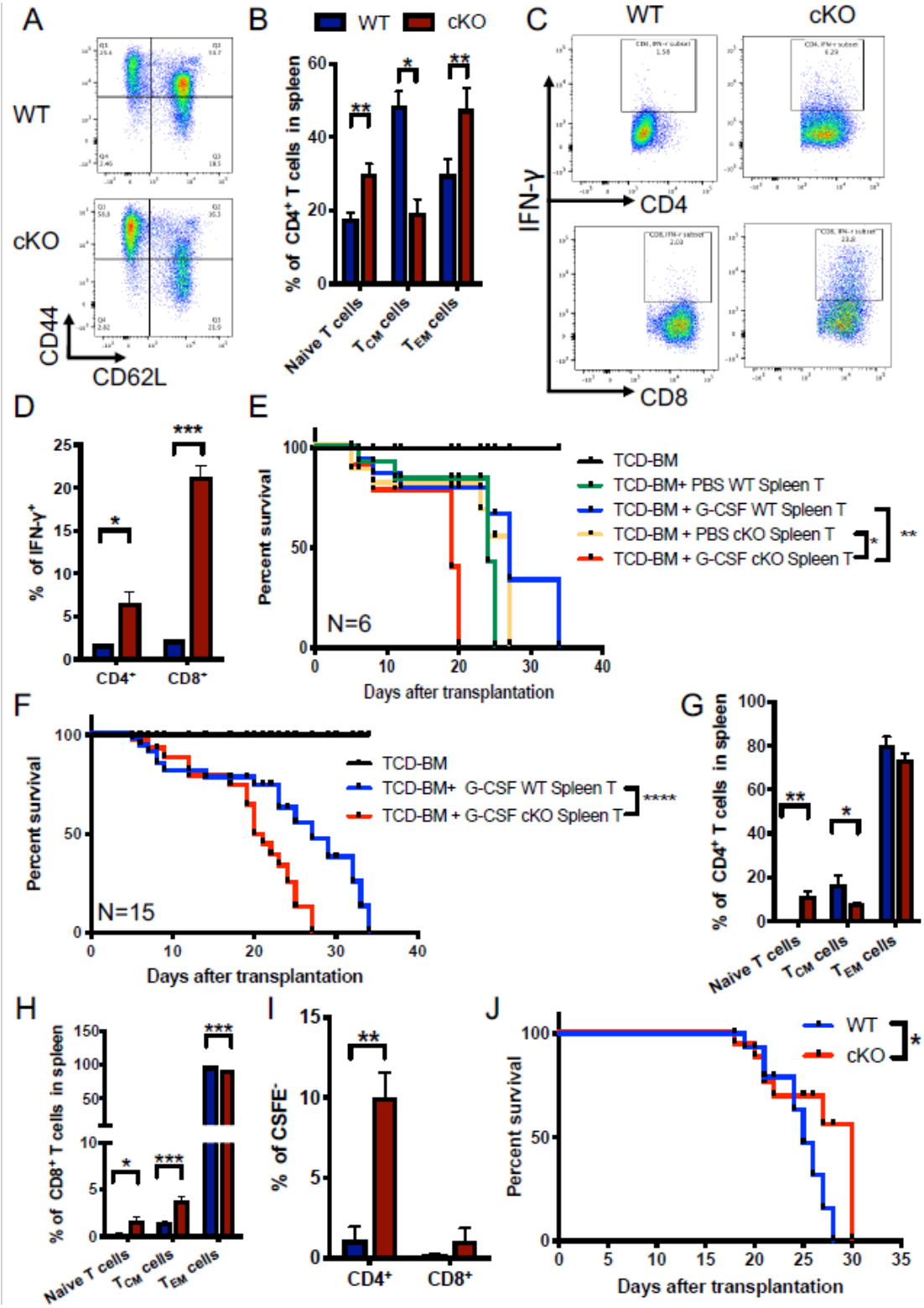

Figure 2

Socs1 is essential for G-CSF protecting recipient mice from GVHD (A-B) Representative flow cytometry results (A) and percentages (B) show the CD62L and CD44 expression levels on CD4+ and CD8+ T cells from the spleens of WT or cKO mice. Naïve T cells: CD62L+CD44-; Central memory T cells (TCM): CD62L+CD44+; Effector memory T cells (TEM): CD62L-CD44+. The experiment was repeated at least 3 times, with 4-6 mice per group. (C-D) Representative flow cytometry results (C) and percentages (D) show

the IFN-γ secretion level of CD4+ and CD8+ T cells from the spleens of WT or cKO mice. The experiment was repeated at least 3 times, with 4-6 mice per group. (E) Survival curves of GVHD mouse models. A total of 5×106 TCD-BM from WT mice treated with PBS and 3×106 T cells from the spleens of the respective treated donor mice were transplanted into the corresponding recipient mice (6 mice per group). (F) Survival curves of GVHD mouse models. A total of 5×106 TCD-BM from WT mice treated with PBS and 2×106 T cells from the spleen of the respective treated donor mice were transplanted into the corresponding recipient mice (15 mice per group). (G-H) Flow cytometric analysis of the CD62L and CD44 expression levels on donor-derived CD4+(G) and CD8+(H) T cells in the spleens of recipient mice. (I) CSFE analysis showed the proliferation ability of donor-derived T cells in the spleen of recipient mice. (J) Survival curves of MLL-AF9 leukemia cells transplanted into nonirradiated cKO (7 mice) or WT (13 mice) recipient mice. Error bars represent the mean ± SEM, ***P<0.001, **P<0.01, *P<0.05.

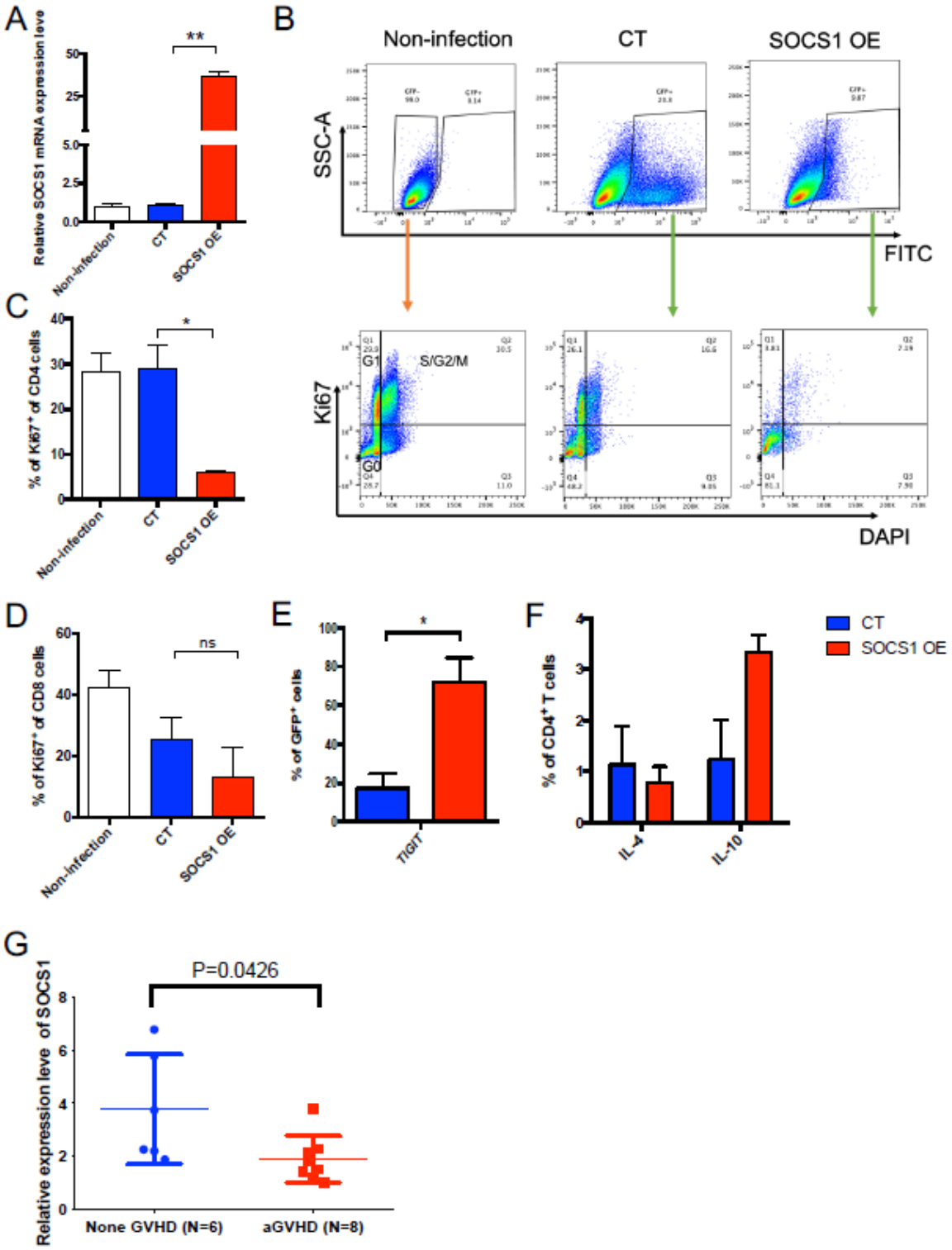

Figure 3

High expression level of SOCS1 impairs T cell proliferation and decreases aGVHD occurrence. (A) SOCS1 was overexpressed by lentivirus in CD3+ T cells from healthy donor bone marrow. Quantitative real-time RT-PCR was used to detect SOCS1 expression levels. (B) Flow cytometric analysis of proliferation in GFP+ cells. (C-D) Percentage of Ki67+ cells in CD4+ cells (C) or CD8+ cells (D). (E) The expression level of TIGIT detected by flow cytometry. (F) IL-4 and IL-10 secretion levels in GFP+ CD4+ T cells. (G) SOCS1

expression level in CD3+ T cells from patients with aGVHD and patients without aGVHD in the same period after allo-HSCT. Error bars represent the mean ± SEM values from 3 independent experiments, *p<0.05, **p<0.01.

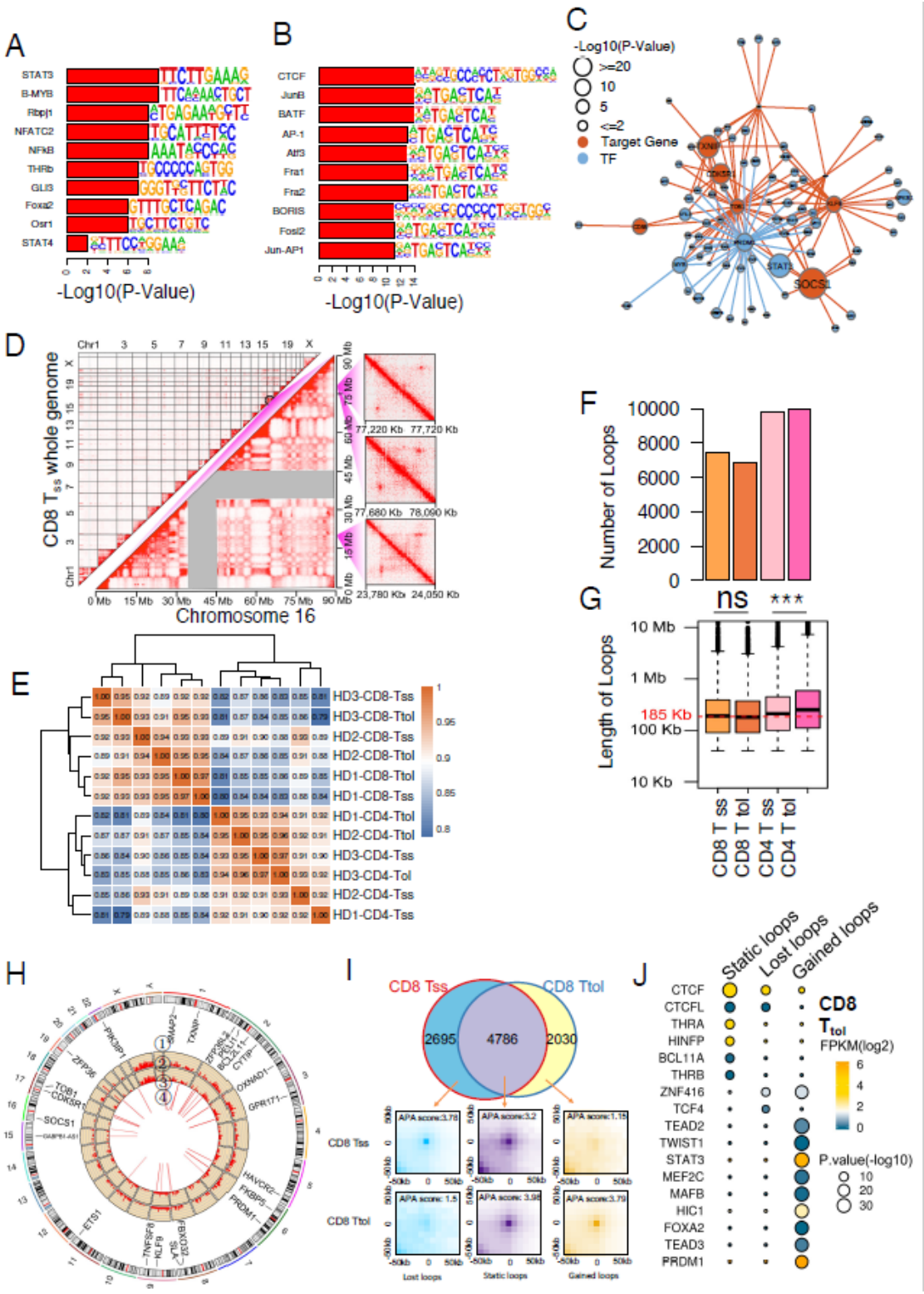

Figure 4

G-CSF regulates target gene expression by chromatin structure alteration. (A) Motif results predicted by HOMER software to have increased chromatin accessibility in CD8 Ttol compared with CD8 Tss cells. (B)

Motif results predicted to have decreased chromatin accessibility in CD8 Ttol compared with CD8 Tss cells. (C) The regulatory network map of highly expressed genes and enhanced transcription factors in CD8 Tss and CD8 Ttol cells. Red dots represent transcription factors, and purple dots represent target genes. The regulatory relationships between transcription factors and genes are based on Yan et al. 17. (D) High-resolution maps of 3D genome structures. Top left: Whole-genome Hi-C interaction matrix of CD8 Tss cells. Bottom right: Hi-C interaction matrix of chromosome 16 of CD8 Tss cells. Right: Examples of three loop structures. (E) Correlations of Hi-C matrices in all samples using HiCRep's SCC scores 18. (F) The number of loops. (G) The length of the loops. Consistent with previous reports, the median loop length was 185 kb (red dotted line), and the loop length of the CD4 cells increased significantly (median length: CD8 Tss cells, 190 kb; CD8 Ttol cells, 180 kb; CD4 Tss cells, 210 kb; CD4 Ttol cells, 340 kb). (H) Highly expressed genes in the loop anchor region of CD8 Ttol compared to CD8 Tss. Of the 55 upregulated genes, 29 were located in the anchor region of the loop. From the outer circle to the inner circle: : gene name; : gene expression levels in CD8 Ttol (from RNA-seq data); : chromosome accessibility from ATAC-Seq in CD8 Ttol; red lines: chromatin loops overlap with genes. (I) Venn diagram of CD8 Tss and CD8 Ttol chromatin loops. APA analysis was performed on the three types of loops in the Venn diagram to verify the reliability of each type of loop. (J) Motif results predicted by HOMER software to have different types of loops in CD8 Ttol cells. CTCF is the transcription factor most significantly enriched in static loops. This finding is consistent with the existing literature.

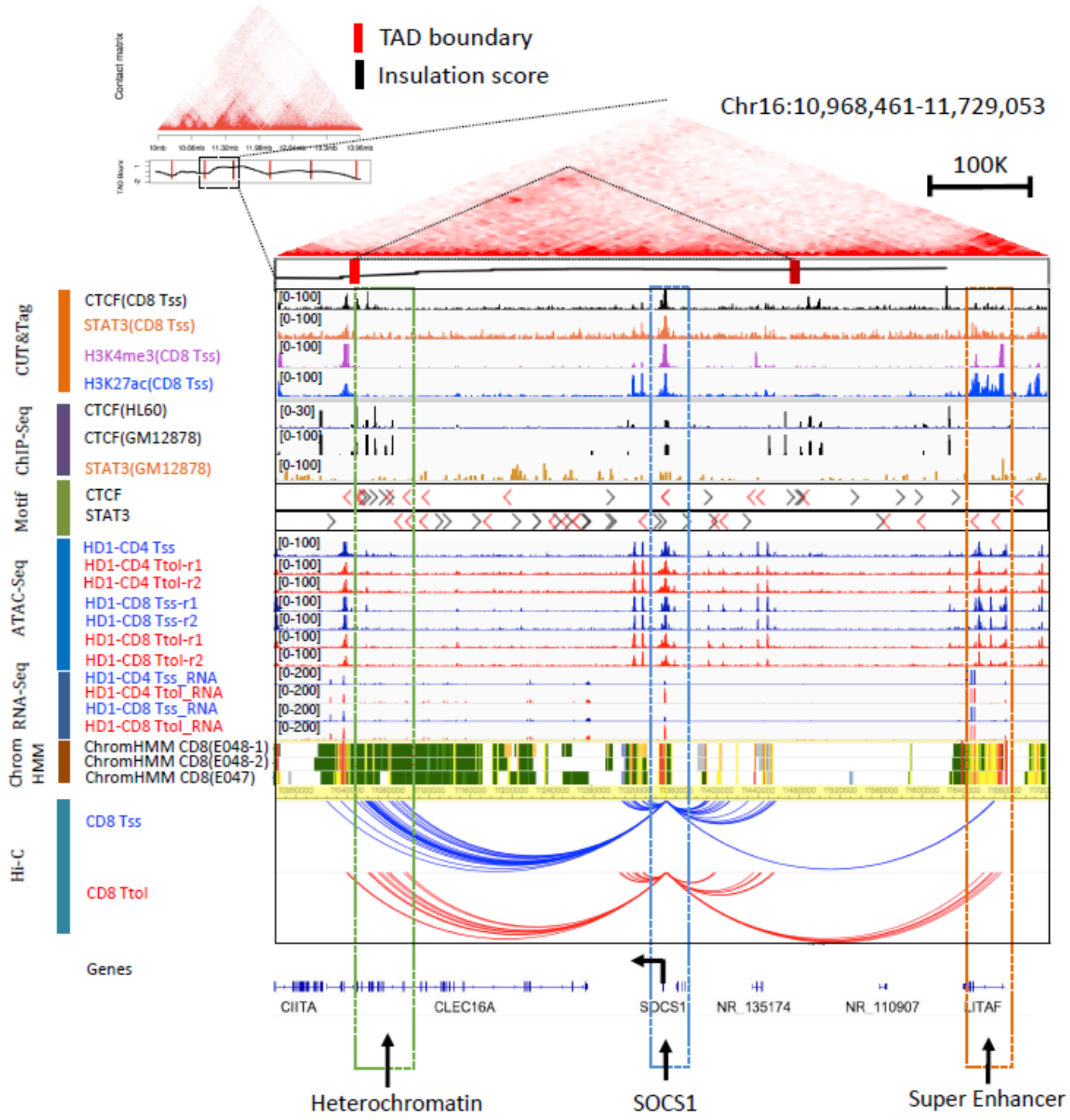

Figure 5

STAT3 regulates SOCS1 expression by 3D genome and chromatin accessibility. Top left: Hi-C interaction matrix of a region (chr16: 10 Mb-14 Mb) in CD8 Tss cells shows the TAD boundaries around the SOCS1 gene. Top: Hi-C interaction matrix, bottom: TAD boundaries (vertical bars) and insulation scores. Bottom right: Genome browser view of CTCF and STAT3 binding sites, motifs, histone modifications, chromatin accessibility, gene expression chromatin states and 3D genome interactions around the SOCS1 gene in CD8 T cells. In the chromatin state line, white represents silenced regions. Green represents chromatin

with weak transcription. Yellow represents strong enhancers. The green box represents the region of chromatin with reduced interactions with SOCS1 after G-CSF mobilization. The yellow box represents the region of chromatin with increase interactions with SOCS1 after G-CSF mobilization. The blue box represents the promoter region of SOCS1.

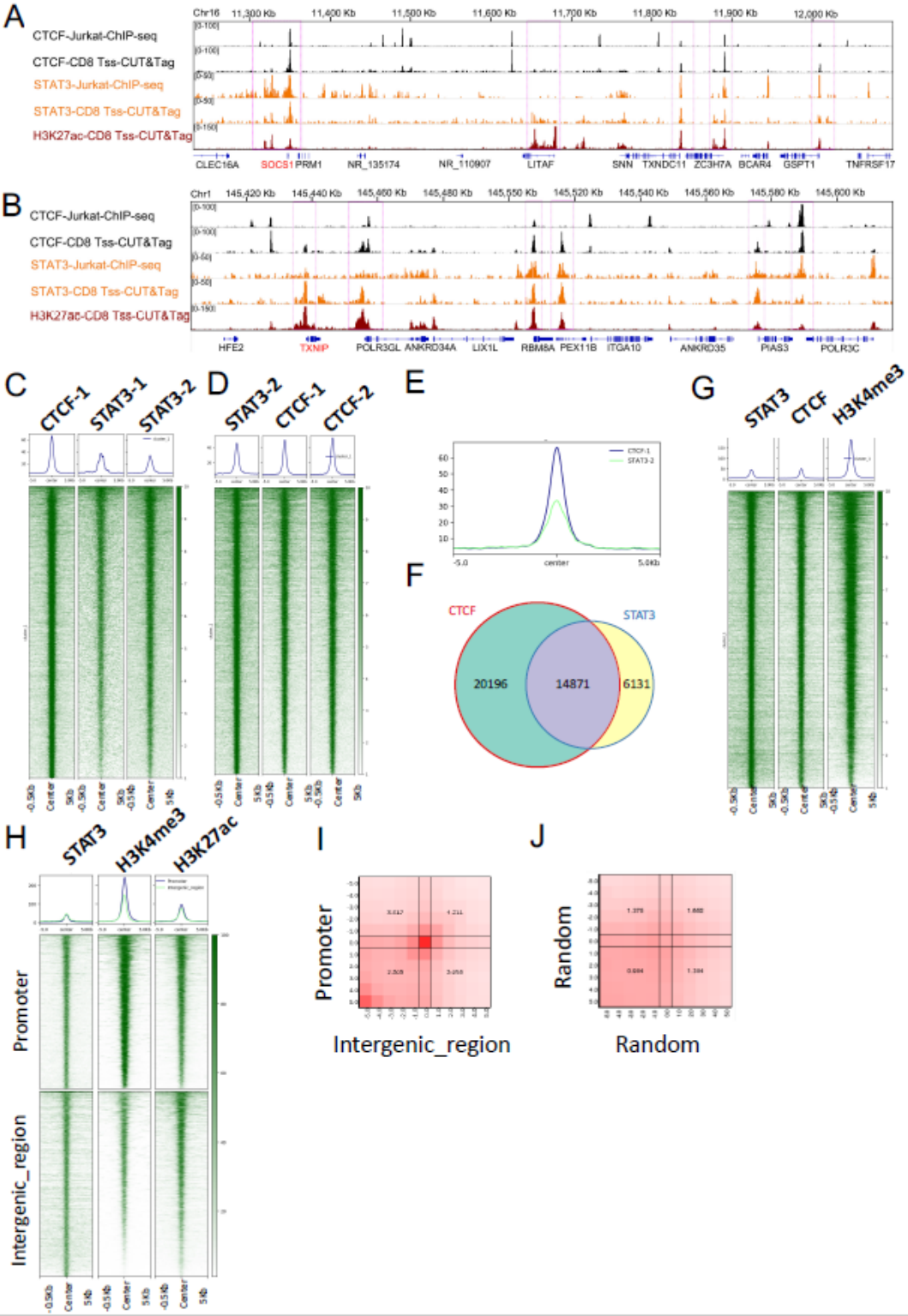

Figure 6

STAT3 and CTCT are colocalized in the whole genome, and STAT3 mediates the spatial interaction between enhancers and promoters. (A-B) UCSC browser views showing histone modifications and transcription factor (TF) binding sites of SOCS1 (A) and TXNIP (B) in Jurkat and CD8 Tss cells determined using ChIP-seq and CUT&Tag data. The pink dotted boxes represent sites where the two transcription factors are colocalized. (C) Heatmaps displaying whole-genome STAT3 and CTCF colocalization in CD8 Tss cells according to CUT&Tag data (the top 5000 CTCF peaks in CD8 Tss cells). (D) Heatmaps displaying whole-genome STAT3 and CTCF colocalization in CD8 Tss cells according to CUT&Tag data (the top 5000 STAT3 peaks in CD8 Tss cells). (E) Aggregate plot of CTCF binding (blue line) and STAT3 binding (green line) at ± 5.0 kb from the CTCF peaks in CD8 cells. (F) Venn diagram showing the overlap between CTCF peaks (red) and STAT3 peaks (blue) in CD8 Tss cells. $p < 1e{-}10$, hypergeometric test. (G) Heatmaps displaying STAT3 occupancy and active promoters (the top 5000 STAT3 peaks in CD8 Tss cells). (H) The peaks of STAT3 binding are classified as belonging to two clusters. The first cluster is the promoter region, which overlaps with the promoters of all genes (± 1 kb around the transcription start site), and the second represents intergenic regions. (I) Heatmap of the interaction between the promoter region and the intergenic region in the spatial interaction between enhancers and promoters. (J) A random selection of the same number of enhancers and promoter peaks has no significant spatial interaction.

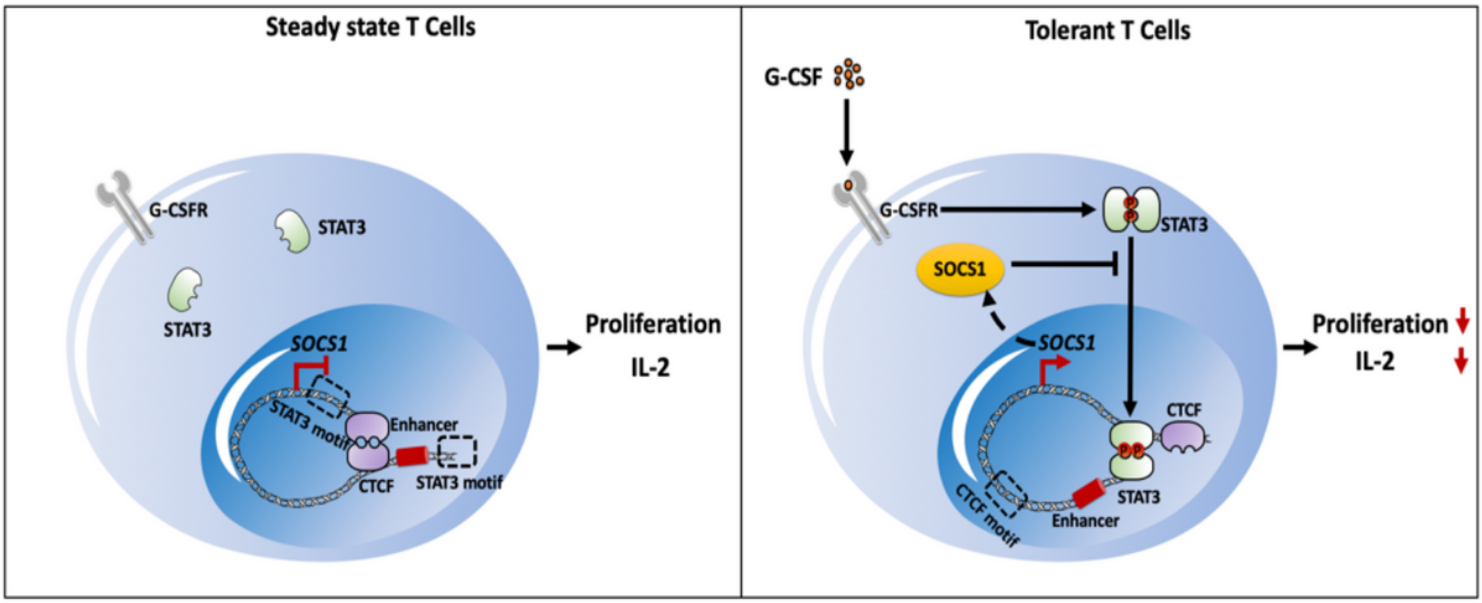

Figure 7

A regulatory model of G-CSF/STAT3/SOCS1 pathway of in vivo induction of human T cell tolerance. G-CSF activated G-CSFR on steady state T cells, leading to activation of STAT3. STAT3 mediated the formation of a new chromatin loop between the SOCS1 promoter and upstream superenhancers, accompanied by the disruption of the CTCF loop between the SOCS1 promoter and downstream heterochromatin. The new chromatin loop upregulated the expression level of SOCS1. SOCS1 further inhibited STAT3 phosphorylation via negative feedback loop. High expression of SOCS1 inhibited T cell proliferation and cytokine secretion, which induced T cells into tolerance state.

Supplementary Files

This is a list of supplementary files associated with this preprint. Click to download.

- 20200107SupplementalFigures.pdf